PAPER

Check for updates

A study on the tribological property of MoS₂/Ti–MoS₂/Si multilayer nanocomposite coating deposited by magnetron sputtering

Ning Kong, [ID] *[a] Boyu Wei,[a] Dongshan Li, [ID] [ab] Yuan Zhuang,[c] Guopeng Sun[c] and Bo Wang[c]

Pure MoS₂ coatings are easily affected by oxygen and water vapor to form MoO₃ and H₂SO₄ which cause a higher friction coefficient and shorter service life. In this work, five kinds of MoS₂/Ti–MoS₂/Si multilayer nanocomposite coatings have been deposited by using unbalanced magnetron sputtering with different modulation period ratios. The tribological tests and nano-indentation experiments have been carried out in order to study the tribological and mechanical properties of the multilayer nanocomposite coating. The results show that the hardness and internal stress of the multilayer nanocomposite coatings are superior to those of the pure MoS₂ coating. The polycrystalline columnar structures are effectively inhibited and the coating densification increases due to the multilayer nanostructure and the doped elements of Ti and Si. The nanocomposite coating with a modulation period ratio of 100 : 100 shows the lowest friction coefficient and wear rate. The multilayer nanocomposite coatings exhibit excellent tribological property under a heavy constant load. Interfaces in multilayer nanostructure coating is able to hinder the dislocations motion and the crack propagation. The doped elements of Ti and Si with nano-multilayer structure enhances the mechanical and tribological properties of MoS₂ coating. This study provides guidelines for optimizing the mechanical and tribological properties of MoS₂ coating.

1. Introduction

Solid lubricant coatings present advantages of low friction coefficient, low wear rate, high reliability and long service life compared with the conventional materials and lubricants, especially in harsh application conditions.[1,2] Transition metal disulfides compounds (TMDs), such as MoS₂ with the unique hexagonal layer structure, are universally used as solid lubricants in the vacuum condition and inert gas environment.[3–9] The excellent tribological property of MoS₂ derives from the unique structure which is similar to the multilayer structure of graphite. In molecular layer of MoS₂, the Mo atoms and S atoms are combined by strong covalent bond interactions, while there is only a relatively weak van der Waals force in the interlayer.[10,11] The tangential sliding is easy to occur between the layers of MoS₂, resulting in excellent self-lubricating property with low friction coefficient.[12,13] MoS₂ coating could be deposited by magnetron sputtering and widely used in the dry air environment, vacuum and space field.[14–17] However, the columnar crystal and loose structures can be easily formed during the

deposition process of pure MoS₂ coating, which reduce the surface hardness and wear durability of coating.[13] Meanwhile, these structures increase the chemical activity to water vapor and oxygen of pure MoS₂ coating. The hard particles (MoO₃) and acidic material (H₂SO₄) form, which aggravate the wear and corrosion of the substrate. It may lead to a failure of pure MoS₂ coating with these defects.[18]

Many researchers have made a lot of efforts to enhance the environmental suitability and service life of MoS₂ coating in order to widen its application range coating. During the deposition growth process of MoS₂ coating, there are two main initial orientations of crystallites. One crystallite is which the basal plane is parallel to the substrate, and the other is perpendicular to the substrate.[19] The MoS₂ crystallites which is parallel to the substrate is predominated at the initial stage of the deposition process.[20] Researches show that when the MoS₂ orientation is parallel to the substrate with a basal plane orientation (002), the tribological property, density of the structure and oxidation resistance will be better than other orientations or random orientation.[21] But as the deposition process continues, the MoS₂ crystallites which is perpendicular to the substrate grows with an unconstrained status.[7,16] Eventually, the MoS₂ single-layer coating is developed to a porous microstructure (columnar crystal structures). MoS₂ multilayer nanocomposite coating shows a lower friction coefficient and wear rate than single-layer coating in moist condition.[22,23] On the one hand, the multilayer

[a]School of Mechanical Engineering, University of Science and Technology Beijing, Beijing, 100083, China. E-mail: kongning@ustb.edu.cn

[b]State Key Laboratory of Solid Lubrication, Lanzhou Institute of Chemical Physics, Chinese Academy of Sciences, Lanzhou, 730000, China

[c]Beijing Institute of Spacecraft System Engineering, Beijing 100094, China

nanostructure can impede the growth of the columnar crystal structures, the motion of the dislocations and the propagation of crack of MoS_2.[24,25] The mechanical and tribological properties of MoS_2 coating is able to be improved. On the other hand, when the MoS_2 layer is at the nanometer scale, the growth orientation of MoS_2 is easier to parallel to the substrate due to the superlattice structures.[26] Therefore, multilayer nanostructure could effectively improve the compactness and orientation of MoS_2, then enhance the oxidation resistance and moisture resistance of MoS_2 coating.[20,24,25] In addition, it is an effective way to improve the tribological property of MoS_2 coating by doping elements in MoS_2 coating. The doped elements[27–31] (including Au, Ag, Cu, Ti, Cr, W) and non-metallic elements[32–35] (including C, Si and N) could effectively enhance the mechanical and tribological properties of MoS_2 coating if properly conducted.

From the present researches, it could be found that the MoS_2 coating with low content of Ti would enhance the mechanical and tribological properties than the pure MoS_2 coating.[29,36] Until now the mechanical and tribological properties of the multilayer nanocomposite MoS_2 coating with the doped elements of both Ti and Si are still not studied in detail. In this work, five kinds of $MoS_2/Ti–MoS_2/Si$ multilayer nanocomposite coatings have been deposited by using magnetron sputtering. The mechanical property, tribological property and microstructure of coatings have been investigated by various characterization methods. This work is to figure out the reasons of the improvement on coating's properties caused by multilayer structure and doped elements of Ti and Si. The effect of modulation period ratio on the tribological property of the multilayer nanocomposite coatings has been revealed as well.

2. Experimental

2.1 The preparation of multilayer nanocomposite coatings

Five kinds of $MoS_2/Ti–MoS_2/Si$ multilayer nanocomposite coatings have been deposited on polished stainless steel (304) and P-type monocrystalline silicon wafer (100) by using the Teer UDP-650 unbalanced magnetron sputtering system in order to study the coating structure and its tribological properties. The magnetron sputtering system includes two MoS_2 targets, one Si target and one Ti target. The purity of all the targets is not less than 99.9%. The size of polished stainless steel (304) is 30 mm × 30 mm × 2 mm, and the size of monocrystalline silicon wafer (100) is 50 mm × 1 mm. Before deposition, the substrates were cleaned in acetone and alcohol bath respectively for 15 minutes by ultrasonic treatment in order to remove the contamination and impurities on substrate surface. Then the substrates were dried in nitrogen. The undefiled substrates were installed on a rotated specimen holder which was placed in the center of the coating chamber in order to ensure the substrates paralleled to the surface of the target. After that, the coating chamber was evacuated by a diffusion pump until the vacuum degree is less than 1.0×10^{-3} Pa. The Argon gas was bubbled into the coating chamber when the pressure reached the required pressure. A bias voltage of −500 V was applied on the substrates for 10 minutes in order to remove the oxides and other impurities on

the substrate surface. Afterwards, the bias voltage of the Ti target was regulated to −70 V. The magnetron current of the Ti target was set to 3.0 A. The Ti intermediate layer was deposited firstly on the substrates before the deposition of the multilayer nanocomposite coatings in order to improve the adhesion property between the substrates and the MoS_2 coating. After the intermediate layer has been deposited, the magnetron current of the Ti target was reduced to 0.8 A, while one of the MoS_2 targets started to work at the same time. The deposition time of MoS_2/Ti was set as 100 s. When the preset time was reached, the Ti and MoS_2 targets lay off, while the Si and the other MoS_2 targets started to work until their preset time was reached. The above process was repeated as shown in Fig. 1. The total deposition time is 2 hours. Five kinds of $MoS_2/Ti–MoS_2/Si$ multilayer nanocomposite coatings with different modulation period ratios have been deposited by changing the deposition time of MoS_2/Si. The coatings with different modulation periods ratios are named as No.1, No.2, No.3, No.4 and No.5, and the parameters are summarized in Table 1.

2.2 Structure and performance characterization of the coatings

The surface roughness of the multilayer nanocomposite coating was measured by Atomic Force Microscopy (AFM). The crystal structures of the coatings were analyzed by D8 Advance X-ray Diffraction (XRD) with a speed of $10° \ min^{-1}$. The cross-section images and nanocrystalline structures were obtained by High Resolution Transmission Electron Microscope (HRTEM). The variation of coating hardness with modulation period was analyzed by the Nano Indenter. The tribological property of the coating was investigated by the ball-on-disc tribometer CSM with 45% relative humidity at 20 °C. A GCr15 ball is chosen as sliding mating materials with 3 mm in diameter. The friction tests were conducted at the constant loads of 2 N and 8 N, respectively. The frequency was 5 Hz, the amplitude was 5 mm, and the reciprocating cycle number was 10 000. The wear rate of coating could be calculated by the eqn (1). The wear rate of each coating is measured for three times to calculate the average value. After the friction tests, the surface micrographs of the coatings and the GCr15 ball were investigated by Scanning Electron Microscopy (SEM). The compositions of the wear debris on the GCr15 ball were analyzed by Energy Dispersive Spectroscopy (EDS).

$$K = \frac{V}{S} \times F \tag{1}$$

where K is the wear rate of coating, V is the wear volume, S is the total distance of sliding, and F is the applied normal load.

3. Results and discussion

3.1 Mechanical performance and microstructure

The surface roughness of the five $MoS_2/Ti–MoS_2/Si$ multilayer nanocomposite coatings with different modulation period ratios on the monocrystalline silicon wafer (100) was observed by AFM, as shown in Fig. 2(a–e). The surface of the No.1 and No.2 coatings are both composed of granulate structures. With
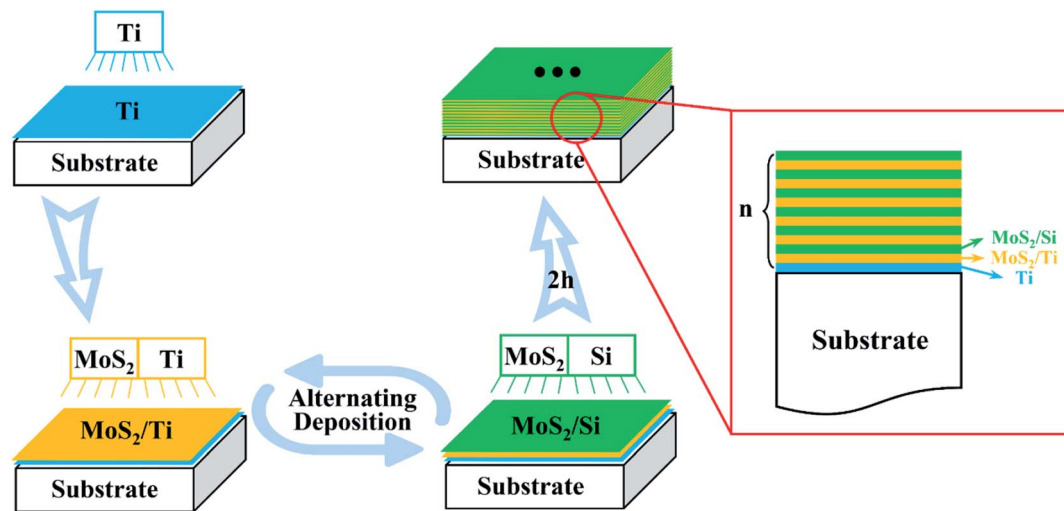
Fig. 1 The structure and depositing process of $MoS_2/Ti–MoS_2/Si$ multilayer nanocomposite coatings.

the extension of the modulation period of MoS_2/Si, the granulate structures of the No.3, No.4 and No.5 coatings reduced as shown in Fig. 2(c–e). The cross-section morphology of each coating was observed by SEM, as shown in Fig. 3. The surface roughness, internal stress and thickness of each coating are summarized in Table 2. The internal stresses of the five coatings were measured by calculating the deformation of the monocrystalline silicon wafer (100) before and after deposition with a stress gauge. The positive value of internal stress is expressed as compressive stress. With increase of the modulation period of MoS_2/Si, the internal stress decreases owing to the growth of the columnar crystal structures is impeded by the alternating deposition process of $MoS_2/Ti–MoS_2/Si$ coatings.[24,25] The metal Ti in the single layer could absorb the plastic deformation during the deposition process, thus the partial residual stress in each film is released.[37]

The hardness of five coatings with different modulation period ratios was performed by Nano Indenter in order to investigate the mechanical properties of the $MoS_2/Ti–MoS_2/Si$ multilayer nanocomposite coatings, as shown in Fig. 4. The multilayer nanostructure and composite phase structure obstruct the growth of the columnar crystal structures and increase the densification of the MoS_2 coating. Therefore, the hardness of each coating increases remarkably compared with the pure MoS_2 coating (around 4.5 GPa).[38] With the extension of the modulation period of MoS_2/Si, the hardness increases first and then decreases. When the modulation period ratio

increases from 50 : 100 to 100 : 100, the hardness of the No.2 coating reaches a maximum value of 7.53 GPa. The hardness of the material is related to the plastic deformation, and the plastic deformation is related to the formation and movement of dislocations in the material. In the multilayer nanocomposite film, the existence of the interlayer interface impedes the formation and movement of dislocations so as to enhance the hardness of the coating.[39] But with further extension of the modulation period of MoS_2/Si, the components between adjacent layers are mixed and the internal diffusion at the interlayer interface increase, resulting in the decrease of the hardness.[40]

The XRD patterns of five kinds of $MoS_2/Ti–MoS_2/Si$ multilayer nanocomposite coatings are shown in Fig. 5. It is reported that the pure MoS_2 coating corresponds to the (002), (100) and (110) crystal face of MoS_2's diffraction peaks are at $2\theta = 13°$, $33°$ and $59°$, respectively.[41,42] In Fig. 5, the diffraction peaks of the (100) and (110) crystal face of the $MoS_2/Ti–MoS_2/Si$ multilayer nanocomposite coatings disappear. The diffraction peaks of the (002) crystal face exists significantly. Therefore, the MoS_2 crystals orient mostly in the (002) plane, which parallels to the surface of the substrate. It could be ascribed to the special alternating layer structure and the existence of abundant interlayer interfaces which hinders the growth of the MoS_2 film in a columnar structure. In addition, there is no obvious diffraction peaks of Ti, Si and their compounds in the XRD pattern. It indicates that the doped elements of Ti and Si mainly exist with a form of amorphous and nanocrystalline in the composite coatings. It is also consistent with the results from previous works.[29] The doped element of Ti is able to improve the oxidation resistance of MoS_2 coating, and low content of Ti would also enhance the mechanical and tribological properties of MoS_2 coatings. The doped elements of Ti and Si also improve the compactness of MoS_2 sublayers, and enhance the oxidation resistance and moisture resistance for the MoS_2 coatings.

HRTEM can effectively analyse short-range order materials while XRD has certain requirements for long-range order (crystal size is larger than 5–10 nm). The cross-section of each

Table 1 Parameters for the deposition of $MoS_2/Ti–MoS_2/Si$ multilayer nanocomposite coatings

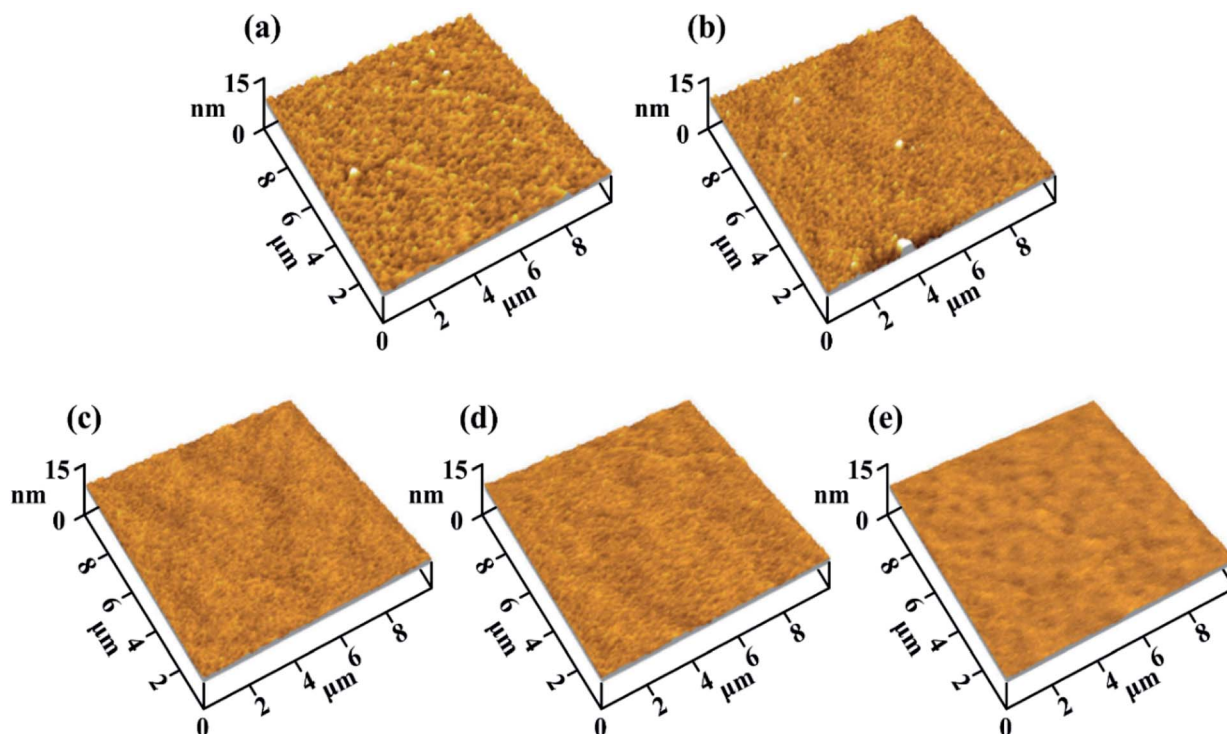| Run no.	No.1	No.2	No.3	No.4	No.5
Magnetron time (s) MoS_2/Si	50	100	150	200	250
Magnetron time (s) MoS_2/Ti	100	100	100	100	100
Magnetron current (A) MoS_2/Ti	0.8	0.8	0.8	0.8	0.8
Magnetron current (A) MoS_2/Si	0.6	0.6	0.6	0.6	0.6

Fig. 2 The surface roughness of MoS_2/Ti–MoS_2/Si multilayer nanocomposite coatings on the monocrystalline silicon wafer observed by AFM.

film has been observed by HRTEM in order to further investigate the microstructure of multilayer nanocomposite coatings at the nanometer scale. The cross-section image of No.4 coating is shown in Fig. 6. The figure clearly shows that the multilayer nanocomposite coating has been grown in a compact, coherent, uniform and obvious layered structure with alternately bright and dark layer during the deposition process. In the nanocomposite coating layer, the nanocrystalline structure of MoS_2, Si and Ti exists with disorganized crystal orientation. It

indicates that the doped elements of Ti and Si effectively hinder the columnar structure growth of MoS_2, which further induces densification, grain refinement and amorphization of the film structure. Meanwhile, the doped elements present in the nanocomposite film as a form of nanocrystals, so the diffraction peaks are not shown in XRD patterns. The doped elements of Ti and Si changes the growth of MoS_2 from columnar structure to an amorphous structure, adjusts the grain arrangement of MoS_2, and further increases the density of MoS_2 coating.
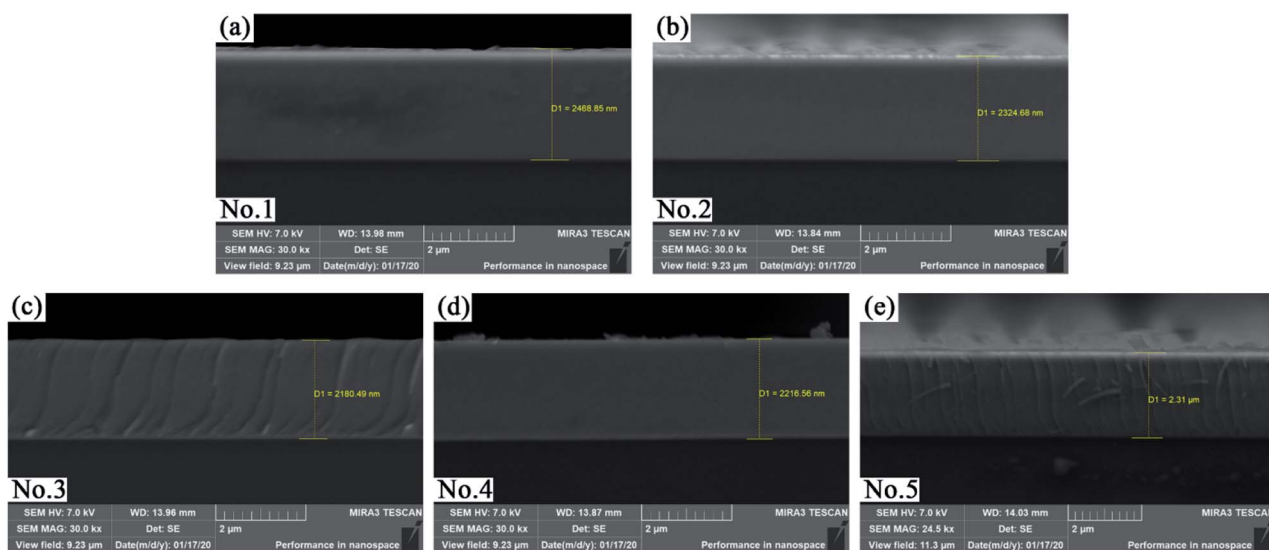

Fig. 3 The cross-section morphology of MoS_2/Ti–MoS_2/Si multilayer nanocomposite coatings by SEM.

Table 2 The surface roughness and internal stress of MoS_2/Ti–MoS_2/Si multilayer nanocomposite coatings

Run no.	No.1	No.2	No.3	No.4	No.5
Surface roughness (nm)	1.55	1.67	0.90	0.86	0.62
Internal stress (MPa)	0.558	0.527	0.520	0.477	0.460
Thickness (μm)	2.47	2.32	2.18	2.21	2.31

3.2 Tribological properties

The friction coefficient curves of MoS_2/Ti–MoS_2/Si multilayer nanocomposite coatings under 2 N and 8 N loads are shown in Fig. 7, respectively. The friction coefficient curve shows a high-to-low trend of running-in process at the initial position due to the high surface roughness of the film in the initial stage of a friction experiment. After the running-in process, the friction coefficient curve reaches to a stable stage. The No.2 nanocomposite coating shows an excellent tribological property with a low friction coefficient under both constant loads of 2 N and 8 N. At a lower constant load, the unevenness of the coating surface presents an obvious influence on the friction interfaces due to the lower contact stress. It also results in the fluctuation of the frictional force and friction coefficient under the combined actions of the abrasive wear and frictional chemical reactions. Meanwhile, the wear debris which are formed during the friction process converts to oxide particles (mainly include MoO_3, TiO_2) due to the frictional chemical reactions.[20,43] The uneven distribution of these oxide particles at the friction interface will be response for the abrasive wear due to their high hardness. When the constant load is 8 N, the coating surface is further compacted by the GCr15 ball, the friction coefficients tend to be stable. Moreover, at a heavy contact load, the contact stress between the two contact surfaces increases. The contact condition tends to be stable. It also reduces the water vapour and oxygen at interface. The frictional chemical reactions could be reduced on the formation of MoO_3 and TiO_2. It will also result in a lower and more stable friction coefficient.[44] The distance between the two contact surfaces decreases with the increase of contact load. The water vapor and oxygen which adsorbed on the coating surface reduces, which leads to a low

and stable coefficient of friction. The average friction coefficient and wear rate of MoS_2/Ti–MoS_2/Si multilayer nanocomposite coatings are shown in Fig. 8 under the constant loads of 2 N and 8 N. It can be seen that the average friction coefficient and wear rate firstly decrease and then increase with the extension of the modulation period of MoS_2/Si. The tribology property of No.2 nanocomposite coating is excellent than that of other coatings with a friction coefficient around 0.0432 and wear rate of 3.22×10^{-7} mm^3 N^{-1} m^{-1} under the load of 8 N. It indicates that the proper modulation period ratio could greatly improve the tribological property of MoS_2 coatings.

The surface micrographs of coatings and the GCr15 ball have been observed by SEM in order to further understand the friction and wear mechanism of the MoS_2/Ti–MoS_2/Si multilayer nanocomposite coatings. The surface micrographs of No.1, No.2 and No.4 films under different constant loads are shown in Fig. 9. When the constant load is 2 N, there are plenty of wear debris and shallow grooves on the surfaces of the multilayer nanocomposite coating along the sliding direction. Blocky flaking occurs on the worn surface as well, as shown in Fig. 9(a)–(c). As the analysis above, the hard particles have been formed due to the frictional chemical reactions between the frictional contact surfaces at a lower load. These hard particles enter the frictional contact surface and cause microscopic cutting motion, so as to produce the hallow grooves on the friction surface. Meanwhile, blocky flaking forms on the worn surface under the action of friction. When the constant load is 8 N, there are large areas of flaking and shallow grooves appear on the worn surface, as shown in Fig. 9(d)–(f). With the increasing constant load, the multilayer nanocomposite coating is further compacted with an obvious plastic deformation region. The micro-cracks appear on the surface of multilayer nanocomposite coating, and further extend under the cyclic alternating friction. When the micro-cracks extend to a certain level, the flaking peel off from the coatings. During friction process, most of the spalled coating materials transfer to the counter surface to form transfer films, which can weaken the friction between the contact pairs. Moreover, some detached materials form hard particles due to the frictional chemical reactions. The
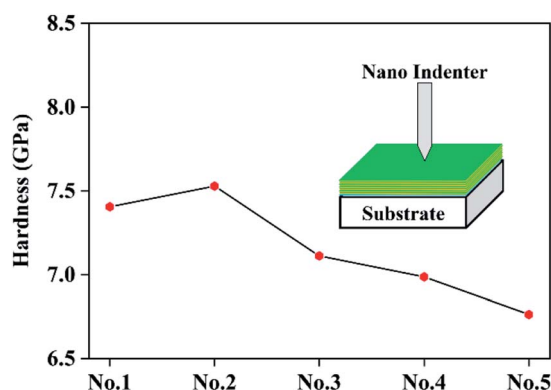
Fig. 4 The hardness of MoS_2/Ti–MoS_2/Si multilayer nanocomposite coatings.
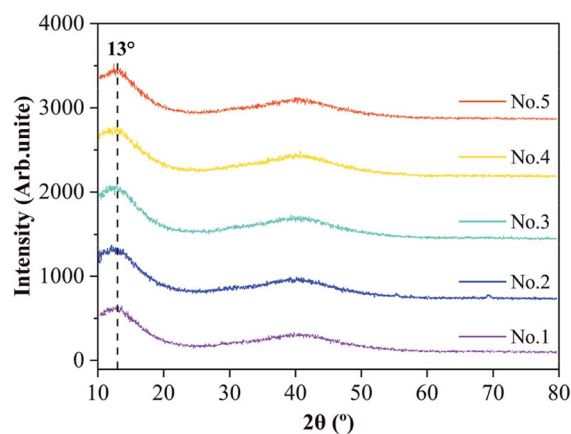
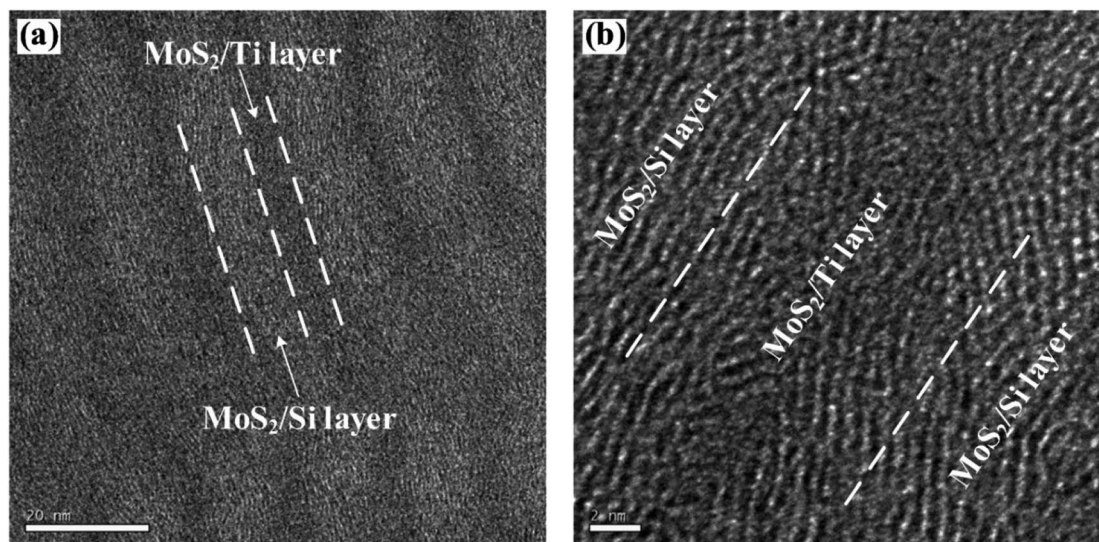**Fig. 5** XRD pattern of MoS_2/Ti–MoS_2/Si multilayer nanocomposite coatings.

Fig. 6 The cross-sectional micrographs of the No.4 MoS$_2$/Ti−MoS$_2$/Si multilayer nanocomposite coating by HRTEM.

sliding of the particles between the frictional contact surfaces results in the formation of shallow grooves. Under a heavy load, the transfer films play a major role in the friction process. It is the reason for the low friction coefficient and low wear rate, as shown in Fig. 8.

The surface micrographs of the GCr15 ball which slides against the No.2 coating and the EDS analysis of the wear scars are shown in Fig. 10. From Fig. 10(a) and (c), the distribution of wear debris is wider and looser under 2 N, while the wear debris distribute densely at a small scale under 8 N. Fig. 10(b) shows the EDS diagram of the compositions of the wear scars on the GCr15 ball under the load of 2 N. There are sharp peaks observed at the positions of Fe and Cr, while the peaks at the Mo and S positions are weak. It indicates that the transfer films have not been formed completely on the surface of GCr15 ball under the load of 2 N. In Fig. 10(d), there are sharp peaks at the Mo and S positions, as well as at the positions of Fe and Cr. The

main component on the wear scar is derived from the transfer films and the GCr15 ball itself under the load of 8 N. Therefore, a thicker and denser transfer film forms on the surface of the GCr15 ball under a heavy load. The presence of the transfer films increases the lubricating ability between the contact interfaces. This result is consistent with the analysis in Fig. 8 above, which the low friction coefficient occurs under a higher load.

3.3 Tribological mechanism of multilayer nanocomposite coatings

Fig. 11(a) shows the microstructure of the pure MoS$_2$ and the MoS$_2$/Ti−MoS$_2$/Si multilayer nanocomposite coatings. There are lots of columnar structure in the pure MoS$_2$ coating, which leads to a loose structure. Contrary, the multilayer nanostructure impedes the growth of the columnar crystal structures. The growth orientation of MoS$_2$ is easier to parallel to the
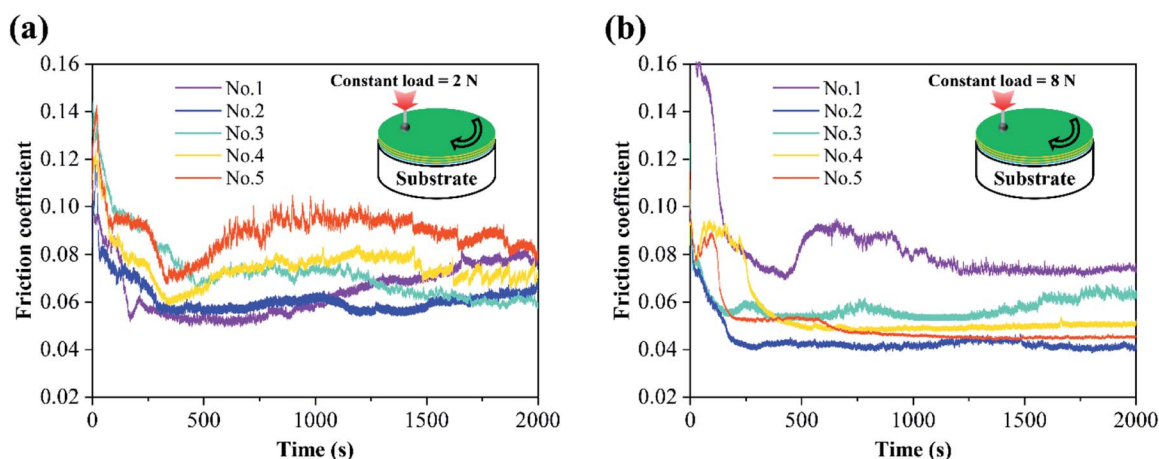

Fig. 7 The friction coefficient of MoS$_2$/Ti−MoS$_2$/Si multilayer nanocomposite coatings under the constant loads of 2 N (a) and 8 N (b), respectively.
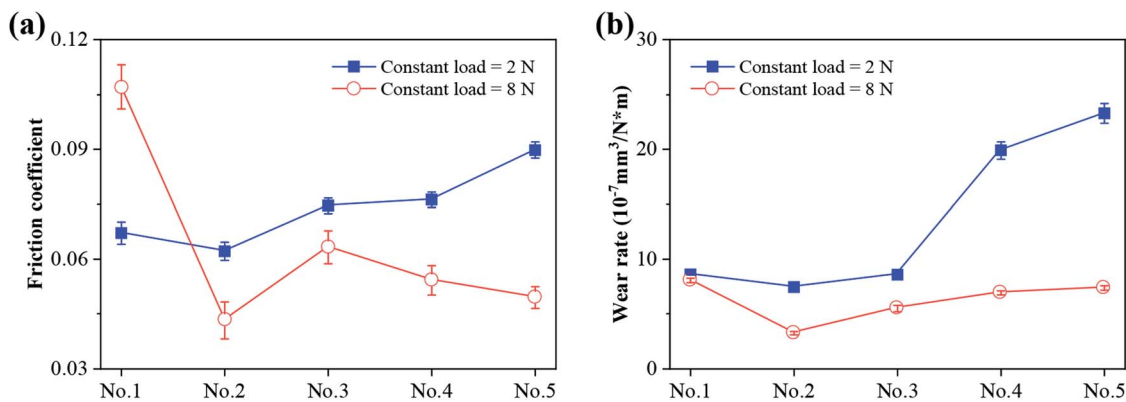
Fig. 8 The average friction coefficient (a) and wear rate (b) of $MoS_2/Ti-MoS_2/Si$ multilayer nanocomposite coatings.

substrate in each coating layer due to the superlattice structures.[26] The multilayer nanostructure could effectively improve the compactness and orientation of MoS_2. It is also responsible to the oxidation resistance and moisture resistance of MoS_2 coating. The difference of the microstructure affects the mechanical property of the two kinds of coatings, as shown in Fig. 11(b). The presence of multilayer nanostructure largely enriches the interface in the coating phases. According to the Hall–Petch (H–P) theory, the interface in multilayer nanostructure coating can hinder the dislocation motion and the crack propagation.[39] As the thickness of layer in the coating further decreases to a nano level, the increase of coating's strength could be interpreted by Orowan mechanism and transmission across interfaces.[40,45] When the modulation period reaches a critical value, a super-hard effect can be produced in the multilayer nanostructure coating. Besides, a crystalline phase of MoS_2 and amorphous phases with the

doped elements exists in the multilayer nanocomposite coating. The crystalline and amorphous phases nanocomposite structure can improve the toughness of the coating.[46] Therefore, the multilayer nanostructure can effectively enhance the mechanical property of MoS_2 coating. The tribology property of MoS_2 coating which is closely related to the mechanical property can be improved accordingly.

MoS_2 is usually used as a soft phase in the composite coating to reduce the friction coefficient between the coating and counterpart surfaces owing to its excellent self-lubricating property.[47] Other hard phase in the composite coating is able to enhance the load capacity and wear resistance of the coating.[48,49] Fig. 12 shows the tribological mechanism of the $MoS_2/Ti-MoS_2/Si$ multilayer nanocomposite coating under different loads. When the set load is 2 N, there are lots of tiny particles from the coating and GCr15 ball on the worn surface due to the shearing action during the friction process. The
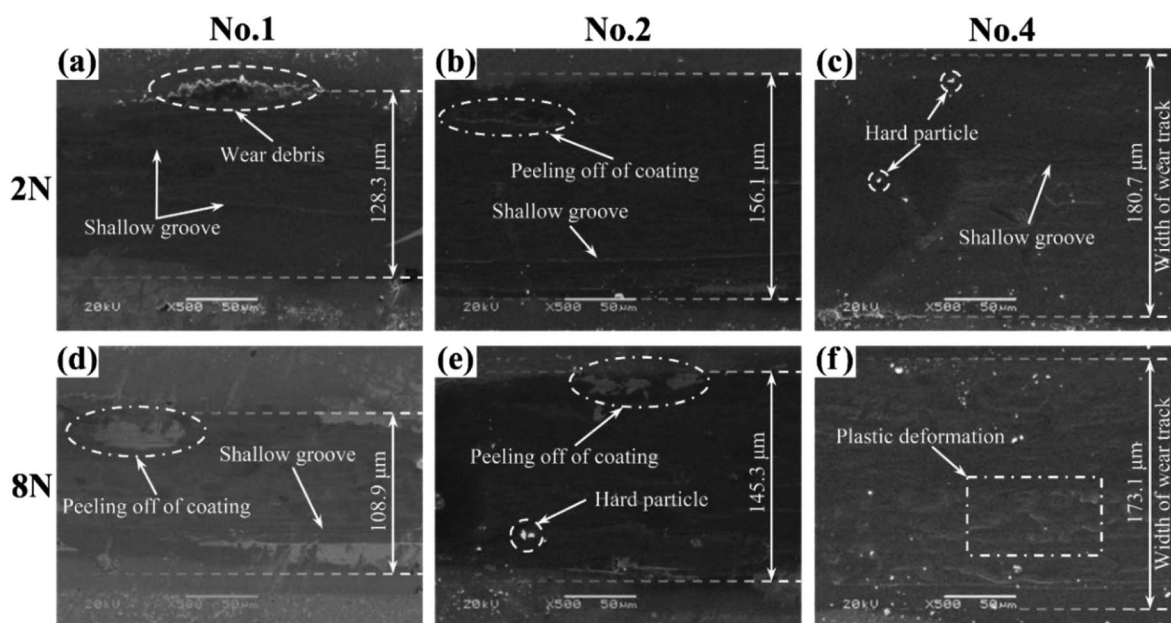

Fig. 9 The surface micrographs of (a) No.1, (b) No.2 and (c) No.4 coatings under the constant load of 2 N; (d) No.1, (e) No.2 and (f) No.4 coatings under the constant load of 8 N.
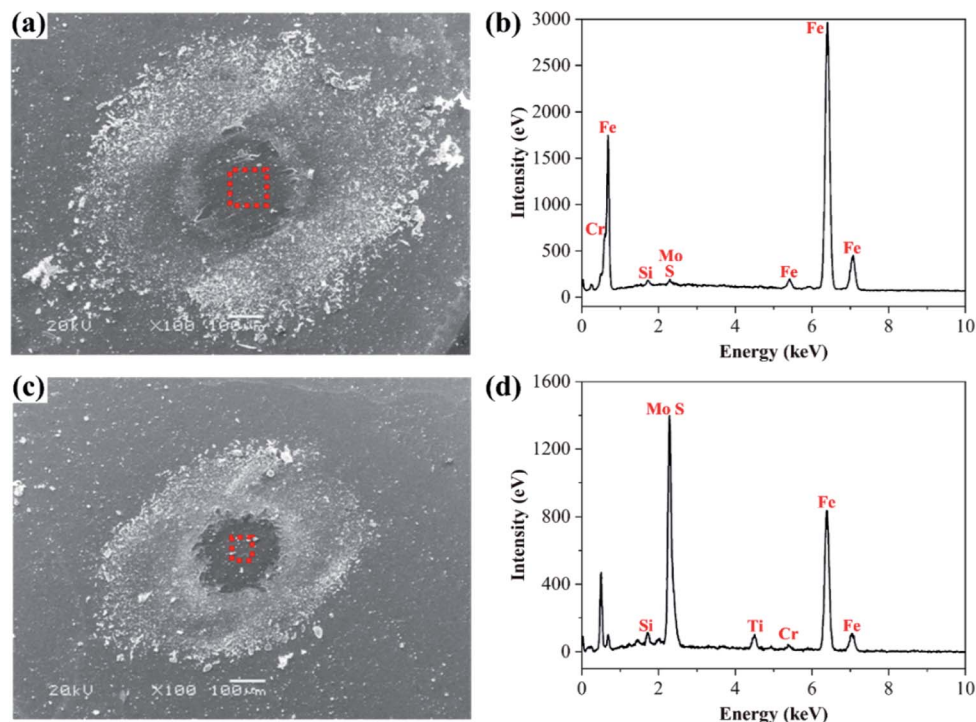
Fig. 10 The surface micrograph of the GCr15 ball (a) and its (b) EDS pattern under 2 N; micrograph (c) and its (d) EDS pattern under 8 N.

chemical activities between MoS_2 particles and water vapor/oxygen increases due to the increase of specific surface area. Then the hard particles (MoO_3) can be form, which aggravate the wear of the coating and GCr15 ball. Under a heavy load, the multilayer nanocomposite coating is further compacted as shown in Fig. 12(b). Some micro-cracks appear on the worn surface due to the cyclic alternating friction and the plastic deformation of the coating. When the micro-cracks extend, the films of the coating peel off and the transfer films form on the counter surface. The quality of the transfer film formed on the counter surface affects the anti-friction property of the coating. A thicker and denser transfer film is easier to form when the constant load is 8 N. It is the main reason for the low friction coefficient and wear rate of the $MoS_2/Ti–MoS_2/Si$ multilayer nanocomposite coating under a heavy constant load.
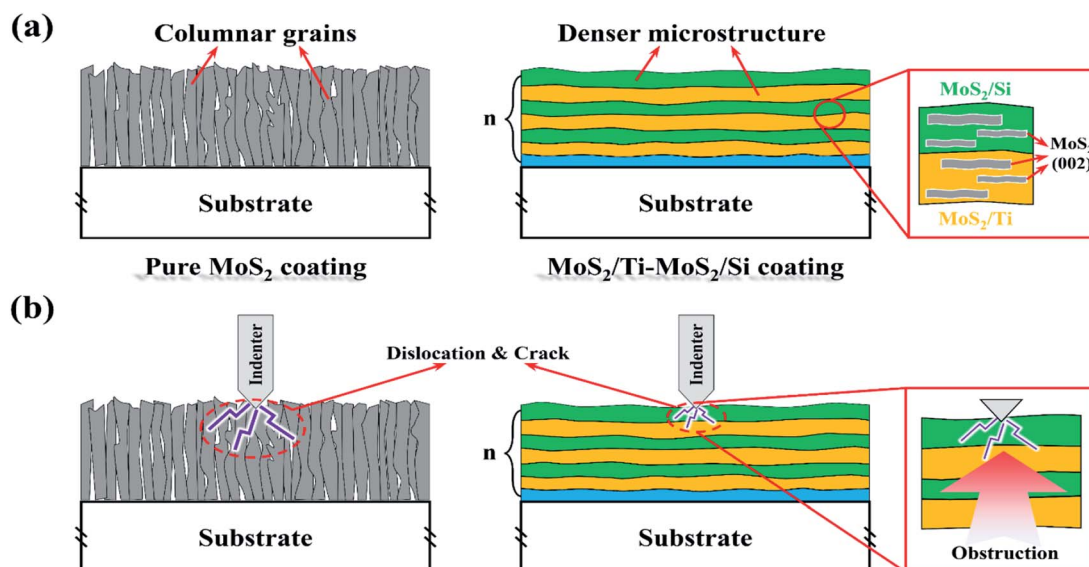

Fig. 11 (a) Schematic illustration of microstructure with coarse columnar structure and denser structure; (b) mechanical property of the pure MoS_2 and $MoS_2/Ti–MoS_2/Si$ multilayer nanocomposite coatings.

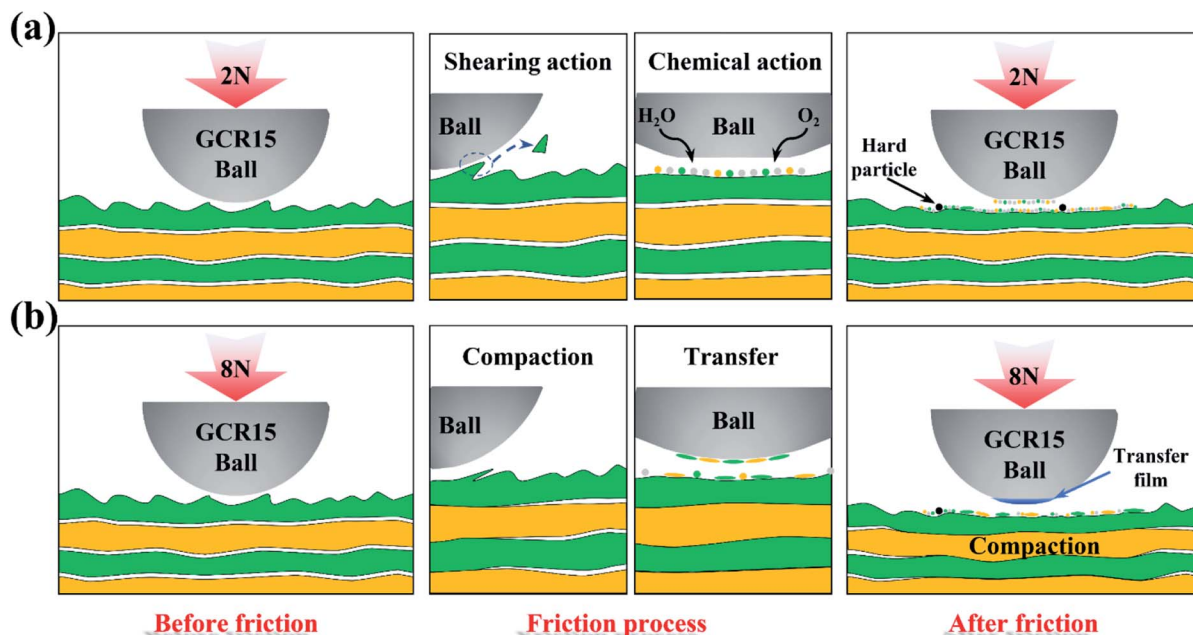Fig. 12 Tribological mechanism of MoS_2/Ti–MoS_2/Si multilayer nanocomposite coatings under with (a) 2 N and (b) 8 N.

4. Conclusion

In this work, five kinds of MoS_2/Ti–MoS_2/Si multilayer nanocomposite coatings have been deposited on polished stainless steel (304) and P-type monocrystalline silicon wafer (100) using the magnetron sputtering system. The mechanical property, tribological property and microstructure of the proposed coatings have been investigated by various characterization methods. The results show that the hardness and internal stress of the nanocomposite coatings are superior to those of the pure MoS_2 coatings. From the microstructure of the nanocomposite coatings, the bright layers and dark layers periodically exist in multilayer coating. The diffraction peaks of the MoS_2/Ti–MoS_2/Si multilayer nanocomposite coatings with (002) crystal face exists significantly while the (100) and (110) crystal face disappear. The doped elements of Ti and Si mainly exist with a form of amorphous and nanocrystalline in the composite coatings. The polycrystalline columnar structures can be effectively inhibited and the densification of film increase due to the multilayer nanostructure and the doped elements of Ti and Si. The multilayer nanocomposite coating with a modulation period ratio of 100 : 100 shows the minimum friction coefficient around 0.0432 and wear rate of 3.22×10^{-7} mm^3 N^{-1} m^{-1} under the load of 8 N. It also exhibits excellent tribological property during the friction process. The tribological mechanism is quite different under 2 N and 8 N. Hard particles from the coating and GCr15 ball spalled on the worn surface due to the shearing and tribo-chemical actions under 2 N and the continuous transfer film cannot be formed. By contrast, when the load reaches to 8 N, the compacted transfer film from the coating materials forms on the contact interfaces with excellent anti-wear and anti-friction performance. Interfaces in multilayer nanostructure coating is able to hinder the dislocations motion and the crack propagation. The multilayer nanostructure and doped elements of Ti and Si enhance the mechanical and tribological properties of MoS_2 coating. This study provides guidelines for optimizing the mechanical and tribological properties of MoS_2 coating.

Conflicts of interest

The authors declare no conflict of interest.

Acknowledgements

References

1 T. W. Scharf and S. V. Prasad, *J. Mater. Sci.*, 2013, **48**, 511–531.
2 C. Donnet and A. Erdemir, *Tribol. Lett.*, 2004, **17**, 389–397.
3 X. Q. Fan, W. Li, H. M. Fu, M. H. Zhu, L. P. Wang, Z. B. Cai, J. H. Liu and H. Li, *ACS Sustainable Chem. Eng.*, 2017, **5**, 4223–4233.
4 M. Yi and C. Zhang, *RSC Adv.*, 2018, **8**, 9564–9573.
5 X. Zhang, J. Wang, H. Xu, H. Tan and X. Ye, *Nanomaterials*, 2019, **9**, 840.
6 A. Gracco, M. Dandrea, F. Deflorian, C. Zanella, A. De Stefani, G. Bruno and E. Stellini, *Nanomaterials*, 2019, **9**, 753.
7 D.-H. Cho, J. Jung, C. Kim, J. Lee, S.-D. Oh, K.-S. Kim and C. Lee, *Nanomaterials*, 2019, **9**, 293.
8 L. Qiao, P. Wang, L. Chai, X. Zhang and W. Liu, *J. Phys. D: Appl. Phys.*, 2015, **48**, 175304.

9 M. C. Simmonds, A. Savan, E. Pfluger and H. Van Swygenhoven, *Surf. Coat. Technol.*, 2000, **126**, 15–24.

10 J. C. Spear, B. W. Ewers and J. D. Batteas, *Nano Today*, 2015, **10**, 301–314.

11 M. Chhowalla and G. A. J. Amaratunga, *Nature*, 2000, **407**, 164–167.

12 N. M. Renevier, J. Hamphire, V. C. Fox, J. Witts, T. Allen and D. G. Teer, *Surf. Coat. Technol.*, 2001, **142**, 67–77.

13 S. Dominguez-Meister, M. Conte, A. Igartua, T. C. Rojas and J. C. Sanchez-Lopez, *ACS Appl. Mater. Interfaces*, 2015, **7**, 7979–7986.

14 W. H. Zhuang, X. Q. Fan, W. Li, H. Li, L. Zhang, J. F. Peng, Z. B. Cai, J. L. Mo, G. G. Zhang and M. H. Zhu, *Carbon*, 2018, **134**, 163–173.

15 J. Pu, S. Ren, Z. Lu and L. Wang, *RSC Adv.*, 2016, **6**, 65504–65517.

16 W. Zhong, S. Deng, K. Wang, G. Li, G. Li, R. Chen and H.-S. Kwok, *Nanomaterials*, 2018, **8**, 590.

17 D. G. Teer, J. Hampshire, V. Fox and V. Bellido-Gonzalez, *Surf. Coat. Technol.*, 1997, **94–95**, 572–577.

18 X. Zhao, G. Zhang, L. Wang and Q. Xue, *Tribol. Lett.*, 2017, **65**, 64.

19 J. Moser and F. Levy, *J. Mater. Res.*, 1992, **7**, 734–740.

20 X. Gao, Y. Fu, D. Jiang, D. Wang, S. Xu, W. Liu, L. Weng, J. Yang, J. Sun and M. Hu, *Surf. Coat. Technol.*, 2018, **353**, 8–17.

21 P. D. Fleischauer, *ASLE Trans.*, 1984, **27**, 82–88.

22 M. R. Hilton, R. Bauer, S. V. Didziulis, M. T. Dugger, J. M. Keem and J. Scholhamer, *Surf. Coat. Technol.*, 1992, **53**, 13–23.

23 L. E. Seitzman, R. N. Bolster and I. L. Singer, *Thin Solid Films*, 1995, **260**, 143–147.

24 L.-n. Zhu, C.-b. Wang, H.-d. Wang, B.-s. Xu, D.-m. Zhuang, J.-j. Liu and G.-l. Li, *Appl. Surf. Sci.*, 2012, **258**, 1944–1948.

25 S. Watanabe, J. Noshiro and S. Miyake, *Surf. Coat. Technol.*, 2004, **188**, 644–648.

26 Z. Zhang, P. Chen, X. Duan, K. Zang, J. Luo and X. Duan, *Science*, 2017, **357**, 788–792.

27 S. M. Aouadi, Y. Paudel, B. Luster, S. Stadler, P. Kohli, C. Muratore, C. Hager and A. A. Voevodin, *Tribol. Lett.*, 2008, **29**, 95–103.

28 J. D. Holbery, E. Pflueger, A. Savan, Y. Gerbig, Q. Luo, D. B. Lewis and W. D. Munz, *Surf. Coat. Technol.*, 2003, **169**, 716–720.

29 S. Ren, H. Li, M. Cui, L. Wang and J. Pu, *Appl. Surf. Sci.*, 2017, **401**, 362–372.

30 M. Cao, L. Zhao, W. Wang, H. Han and W. Lang, *AIP Adv.*, 2019, **9**, 045105.

31 K. Shang, S. Zheng, S. Ren, J. Pu, D. He and S. Liu, *Appl. Surf. Sci.*, 2018, **437**, 233–244.

32 L. Gu, P. Ke, Y. Zou, X. Li and A. Wang, *Appl. Surf. Sci.*, 2015, **331**, 66–71.

33 G. Ma, B. Xu, H. Wang, X. Wang, G. Li and S. Zhang, *Surf. Coat. Technol.*, 2013, **221**, 142–149.

34 A. Nossa and A. Cavaleiro, *Surf. Coat. Technol.*, 2001, **142**, 984–991.

35 S. Banday and M. F. Wani, *Surf. Interface Anal.*, 2019, **51**, 649–660.

36 E. Arslan, F. Bulbul, A. Alsaran, A. Celik and I. Efeoglu, *Wear*, 2005, **259**, 814–819.

37 D. Y. Wang, C. L. Chang, Z. Y. Chen and W. Y. Ho, *Surf. Coat. Technol.*, 1999, **120**, 629–635.

38 X. Wang, Y. Xing, S. Ma, X. Zhang, K. Xu and D. G. Teer, *Surf. Coat. Technol.*, 2007, **201**, 5290–5293.

39 A. Misra, M. Verdier, Y. C. Lu, H. Kung, T. E. Mitchell, N. Nastasi and J. D. Embury, *Scr. Mater.*, 1998, **39**, 555–560.

40 A. Misra and H. Kung, *Adv. Eng. Mater.*, 2001, **3**, 217–222.

41 J. Moser and F. Levy, *Thin Solid Films*, 1994, **240**, 56–59.

42 W. Y. Lee and K. L. More, *J. Mater. Res.*, 1995, **10**, 49–53.

43 H. Li, X. Li, G. Zhang, L. Wang and G. Wu, *Tribol. Lett.*, 2017, **65**, 38.

44 A. K. Kohli and B. Prakash, *Tribol. Trans.*, 2001, **44**, 147–151.

45 J. D. Embury and J. P. Hirth, *Acta Metall. Mater.*, 1994, **42**, 2051–2056.

46 A. Urakami and M. E. Fine, *Scr. Metall.*, 1970, **4**, 667–671.

47 K. Zhang, J. Deng, S. Lei and X. Yu, *Surf. Coat. Technol.*, 2016, **291**, 382–395.

48 W. D. Sproul, *Science*, 1996, **273**, 889–892.

49 H. Holleck, *J. Vac. Sci. Technol., A*, 1986, **4**, 2661–2669.